

# Dynamic Pt-OH•H<sub>2</sub>O-Ag Species Mediate Synergetic Electron and Proton Transfer for Catalytic Hydride Reduction of 4-Nitrophenol at Confined Nanoscale Interface

Meng Ding,<sup>1†</sup> Bing-Qian Shan,<sup>1†\*</sup> Bo Peng,<sup>1</sup> Jia-Feng Zhou,<sup>1</sup> Kun Zhang<sup>\*1,2,3</sup>

<sup>1</sup>Shanghai Key Laboratory of Green Chemistry and Chemical Processes, College of Chemistry and Molecular Engineering, East China Normal University, Shanghai 200062, China;

<sup>2</sup>Laboratoire de chimie, Ecole Normale Supérieure de Lyon, Institut de Chimie de Lyon, Université de Lyon, 46 Allée d'Italie, 69364 Lyon cedex 07, France;

<sup>3</sup>Shandong Provincial Key Laboratory of Chemical Energy Storage and Novel Cell Technology, School of Chemistry and Chemical Engineering, Liaocheng University, Liaocheng, 252059, Shandong, P. R. China.

\* Correspondence: [bqshan\\_ecnu@163.com](mailto:bqshan_ecnu@163.com), [kzhang@chem.ecnu.edu.cn](mailto:kzhang@chem.ecnu.edu.cn) (K.Z.)

## Abstract

The nature of interfacial state and/or bonding at heterogeneous nanoscale surface of bimetals remains elusive. For very classical probe reaction of catalytic hydride catalytic reduction of –NO<sub>2</sub> to NH<sub>2</sub> (herein reduction of 4-NP to 4-AP as an example), three abnormal experimental phenomena cannot be elucidated as such: 1) the hydrogen source of final product of 4-AP is originated from water solvent, rather than NaBH<sub>4</sub> reducer; 2) reverse electron transfer between bimetals was observed, which is resisted to the normal thermodynamic law; 3) even in the absence of any metals, for example just using carbon nanodots as supports, the reaction occurs. These observations indicate that the reduction of –NO<sub>2</sub> groups did not follow the classical metal-centered electron and hydride transfer mechanism, i.e., Langmuir-Hinshelwood (L-H) mechanism. We herein provide strong evidence that, the catalytic hydride reduction of 4-NP to 4-AP is through a completely new surface hydrous hydroxyl species mediated concerted electron and proton transfer process, wherein owing to the space overlapping of p orbitals in hydrous hydroxyl intermediate, an ensemble of interface states are dynamically formed, which could be alternative channels for concerted electron and proton transfer. The main role of second metal of Pt is to regulate the density of surface hydrous hydroxyl intermediate and its interactive strength with metals. This new mechanism not only answers all the abnormal experimental observations above mentioned, but also provides some new insights to water and/or hydroxyl group promoted reaction involving the activation of small molecules (CO<sub>2</sub>, CO, N<sub>2</sub>, H<sub>2</sub>O etc.) in areas of electrochemistry, energy storage and metalloenzyme catalysis.

## Introduction

Bimetallic nanoparticles composed of two different metal elements are universally effective strategies to achieve high activity, selectivity and stability in the redox reaction. In general, the improved performance in bimetallic have

been pervasive attributed to “synergistic effect” arising from Metal-to-Metal direct charge transfer, which may provide an uneven distribution of electrons and make the electron density of one metal greater than another (scheme 1a and 1b). Thus, the theories of d-band model, work function, electronegativity, and electrochemical potential of metal (scheme 1a) were often used to elucidate the working mechanism of bimetal catalysts(1-4). But, the metal-centered electron transfer model does not apply universally, and in some case, even paradoxically, such as, abnormal anti-galvanic reduction of Au-Ag and Co-Fe bimetals(5-7). This strongly indicates that, at nanoscale interface, there must be dark alternative channels for surface electron transfer. Thus, the consideration of interfacial states is necessary.

Increasingly, the solid evidences proved that interfacial hydrous hydroxyl and oxy species at bimetal interface plays a critical role to mediate the surface electron and proton transfer in chemical transformations, in particular for the catalytic conversion of C1 molecules. Mullins and his coworkers observed the involvement of water in oxidizing impinging CO on oxygen atom-precovered Au(111) at low temperatures, and proposed that OH formed from water interacting with atomic oxygen on Au(111) are responsible for the promotional effect in oxidizing CO to produce CO<sub>2</sub> on the surface(8-11). Subsequently, in the water-gas shift (WGS) reaction, a common alkali metal ions stabilized single-site M-O(OH)<sub>x</sub> species on both active and inert supports was identified as real active sites by Flytzani-Stephanopoulos and his coworkers(12-14). Very recently, Gong’s group demonstrated that, not only in the thermal catalytic reaction, also in the CO<sub>2</sub> electrocatalytic reduction (CO<sub>2</sub>RR) the coverage and density of surface hydroxyls at metal nanoscale interface determined the chemical activity and selectivity of CO<sub>2</sub> hydrogenation(15-17). Indeed, the surface hydroxyl group promoted the chemical transformation is not only limited to the activation of small molecules closely related to energy storage, such as CO, CO<sub>2</sub> and water etc.(18), but also extended to bulky organic molecules with high-added value, including propane, substituted nitroarenes and  $\alpha,\beta$ -unsaturated aldehydes(17, 19-26). Thus, all the reported results highlighted the pivotal role of surface hydrous hydroxyl and/or oxy group to regulate the chemical reactivity, but their interactive binding mode and strength with metals, support effect and metal alloy and/or doping effect are not clear(20, 27-32), i.e., the nature of interfacial state and/or bonding at heterogeneous remains elusive.

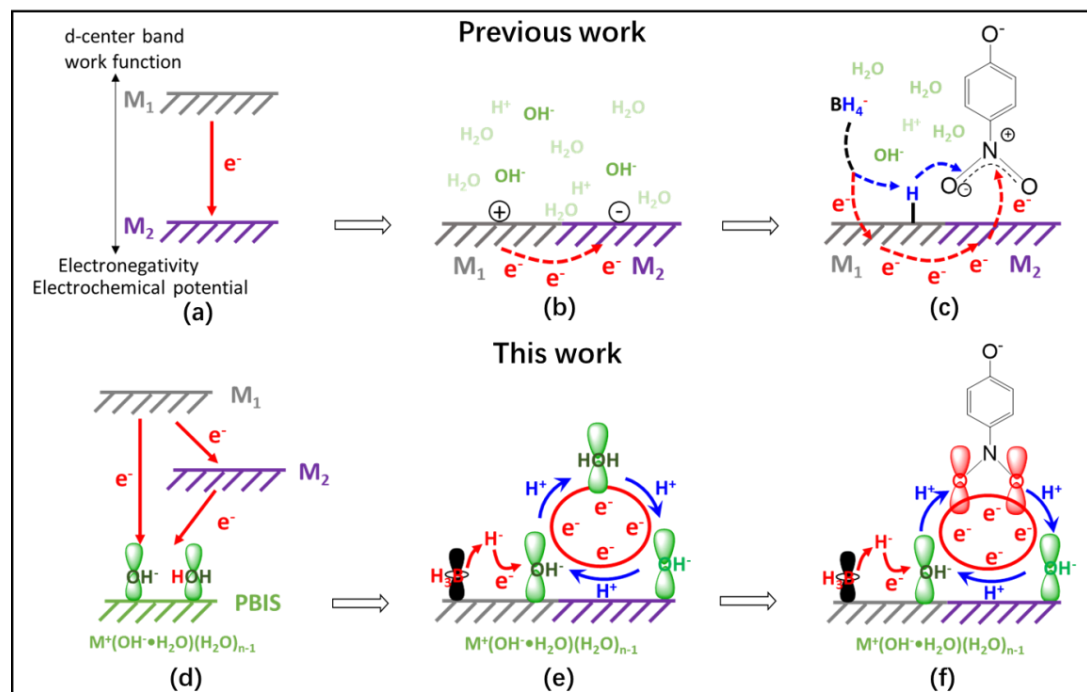
Recently, relying on the combined characterizations of absorption, excitation and photoluminescence spectrum and femto-second time-resolved ultra-fast transient absorption technique, an ensemble of dynamic intermediate states with  $\pi$  bonding characteristic, so called the p band states, stemming from the spatial overlapping of p orbitals of oxygen atoms in the hydrous hydroxyl (OH<sup>-</sup>) and/or oxy species at confined metal or nonmetal

nano-interface, was unambiguously identified, which can be alternative radiation decay pathway for the electron transfer of excited states(33-36). More recently, the p band dominated interfacial electron transfer theory successfully elucidates the reaction mechanism of several typical probe reactions at mono-metal catalysts(21, 22, 31, 37).

Among these probe reactions, the hydride reduction of 4-NP to 4-AP in an aqueous solution using sodium borohydride ( $\text{NaBH}_4$ ) as a hydride source is one of the most widely used model reactions to evaluate the catalytic activity of a large variety of metal NP catalysts. The process of catalysis is general believed to follow Langmuir–Hinshelwood (L-H) mechanism(38, 39), in which  $\text{NaBH}_4$  both as reducing agent and hydrogen source, and the dissociation of B-H bond on the metal surface as well as the formation of metal-H species are key steps (Scheme 1 c). However, in the latest work, the higher reactivity of  $\text{Ag}^+$  than Ag NPs under the same conditions, showed a direct and powerful evidence that the metal surface is not necessary for interfacial electron transfer(21, 22). More recently, the metal-free catalysts, such as graphene quantum dots, are also active for hydride reduction of 4-NP, which further confirmed that metal center was not the catalytic sites for this reaction(40). Thus, the exact role of metals and the hybrid metals to tune the interfacial electron and proton transfer for hydride reduction of 4-NP remains elusive.

Herein, we report a comprehensive study of 4-NP reduction on a series of Pt-Ag bimetallic nanoparticles with different Pt/Ag ratios confined in mesoporous silica nanospheres (DMSNs). The investigations of reaction kinetics demonstrated that, even in the presence of trace Pt (0.25 wt %), the reduction reaction rate of Pt-Ag bimetallic catalyst is 17 times and 2 times higher than that of single metal Pt and Ag catalyst, respectively. Designed isotope labeling experiment of deuterated  $\text{NaBD}_4$  reducer and solvent  $\text{D}_2\text{O}$  coupled with XPS and FT-IR shows the strong evidences that, the catalytic hydride reduction of 4-NP did not follow the traditional metal-mediated interfacial electron transfer pathway (Scheme 1a-c), i.e., classical Langmuir-Hinshelwood (L-H) mechanism, Instead, but follows a completely new interface-state-mediated concerted electron and proton transfer process (Scheme 1d-f)). The optical excitation and photoluminescence spectrum identified the presence of these dynamic interface states, stemming from space overlapping of p orbitals of several O atoms of water-hydroxyl-metal complex  $\{\text{M}^+(\text{OH}\cdot\text{H}_2\text{O})\cdot\text{H}_2\text{O}_{n-1}\}$ . Very interestingly, we found that, the density of hydrous hydroxyl groups and its interacted strength with metal surface not only accelerate the reaction rate of 4-NP reduction, but also promote the ripening of Ag NPs due to the dosing of Pt atoms.

**Scheme 1. Comparison of Different Electron and Proton Transfer and Reaction Mechanisms in Bimetal-Catalyzed Hydride Reduction of 4-Nitrophenol (4-NP) in Aqueous Medium: classical metal mediated hydride and electron transfer mechanism, ie., Langmuir-Hinselwood (L-H) mechanism (Scheme 1a-c); Surface hydrous hydroxyl intermediate mediated concerted electron and proton transfer mechanism (Scheme 1 d-f).**



## Result and discussion

$Pt_xAg_{2-x}$  bimetallic catalysts ( $Pt_xAg_{2-x}@DMSNs$ ) were prepared by a multi-step in-situ nanocrystal seeding-induced-growth (SIG) method with mesoporous silica nanosphere (DMSNs) as a distinctive confinement support (Experiment section in Supporting Information)(41), where  $x$  is metal loading in weight percentage. The composition of the bimetallic catalysts can be tailored over a broad range of values of  $x$  by keeping the total metal content of Pt and Ag of 2% in weight. The combined characterizations by the transmission electron microscopy (TEM) (Fig.1a, Fig. S2), annular dark-field TEM (Fig. 1b) and corresponding elemental mapping (Fig. 1c-1e), confirmed that the  $Pt_xAg_{2-x}$  bimetallic NPs are uniformly distributed throughout DMSNs. Note that DMSNs have small spherical pores ( $\sim 3$  nm) in the dendritic networks (Fig. S1), which provides a unique nanospace for the confinement of the metal NPs(41-44). As a consequence, the size of metal NPs is smaller ca. 2.0 nm in monometallic  $Pt_{2.0}@DMSNs$  and  $Ag_{2.0}@DMSNs$  (Fig. S2). Interestingly, the size of bimetallic NPs is decreased with the increase of Pt content in order of  $Pt_{0.25}Ag_{1.75}@DMSNs$  (7.0 nm) >  $Pt_{0.5}Ag_{1.5}@DMSNs$  (5.0 nm) >  $Pt_{1.0}Ag_{1.0}@DMSNs$  (3.0 nm) >  $Pt_{1.5}Ag_{0.5}@DMSNs$  (2.0 nm), larger than monometallic NPs (2.0 nm), which is consistent with the results of the XRD patterns (Fig. 1f). It means that the introduction of trace amount of Pt greatly promotes the nucleation and growth of Ag NPs, which never reported before.

Coupling with the reaction data of 4-NP reduction, the reason for the role of Pt to promote the growth of Ag mediated by interface states will be discussed later.

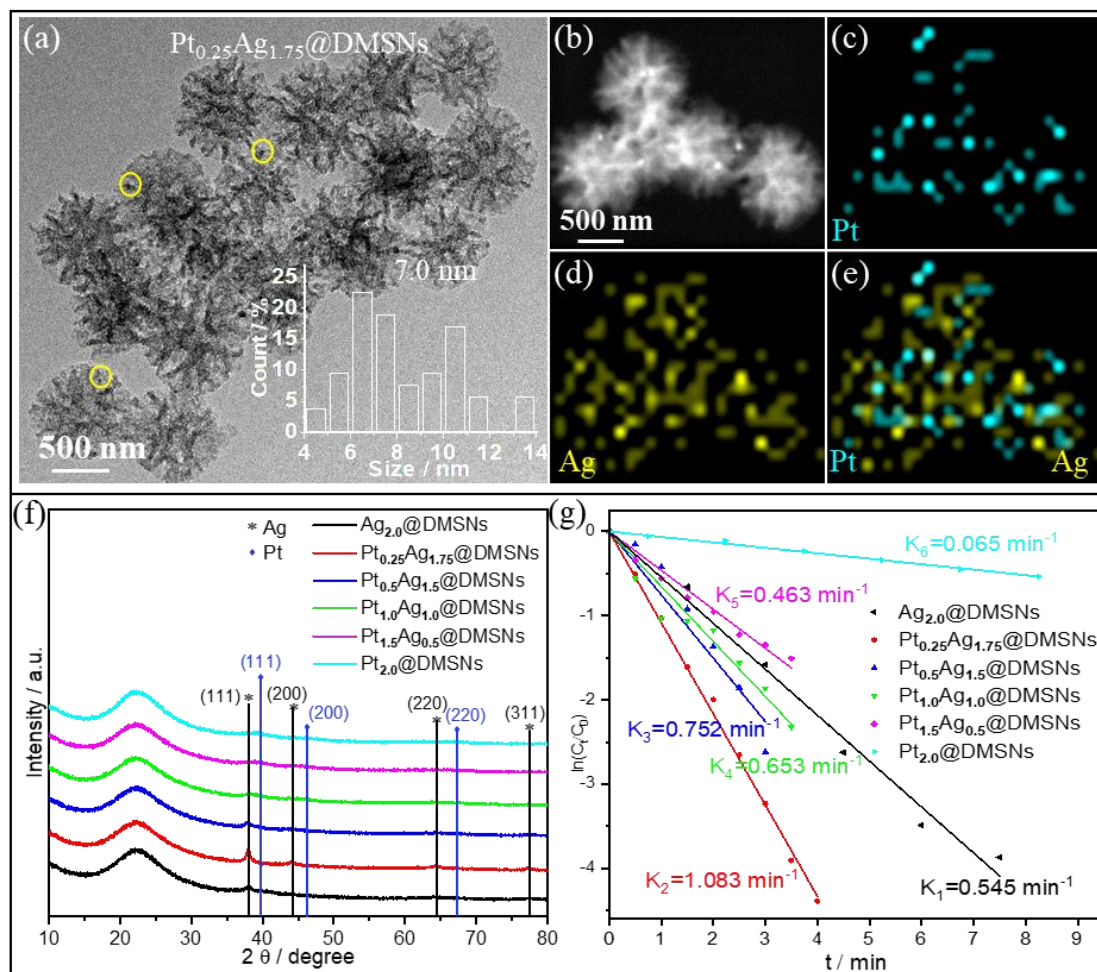


**Figure 1.** TEM images of Pt<sub>0.25</sub>Ag<sub>1.75</sub>@DMSNs (a). The inset is the corresponding particle size distribution. HAADF-STEM (b) micrograph of Pt<sub>0.25</sub>Ag<sub>1.75</sub>@DMSNs and the corresponding STEM-EDX mappings of Pt (blue) and Ag (yellow), respectively. The XRD patterns (f) and catalytic reactivity (g) of Pt<sub>0.25</sub>Ag<sub>1.75</sub>@DMSNs for the reduction of 4-NP with NaBH<sub>4</sub>.

To elucidate the surface composition/elemental chemical states of the prepared Pt<sub>x</sub>@DMSNs with different metal loadings, the XPS studies were conducted and the binding energy (BE) values referred to Pt 4f<sub>7/2</sub> peak are analyzed (Fig. S3, Table S1). The bulk Pt<sup>0</sup> (71.2 eV) and Pt<sup>2+</sup> (72.7 eV) were both found in Pt<sub>2.0</sub>@DMSNs and Pt<sup>0</sup> is the main component (74.5%). However, the Pt is more electron-deficient in Pt<sub>0.25</sub>@DMSNs with only Pt<sup>2+</sup> (72.5 eV) species appeared, which can not reduce Ag<sup>+</sup> to Ag NP. Notably, the binding energy (BE) centered at 72.5 eV is ascribed to the interaction between Pt and hydroxide(24, 45, 46). Very recently, a series of innovative and important work confirmed the existence of new interface states (PBIS) stemming from the spatial overlapping of p orbitals of surface ligand atoms on the surface of metal

nanoclusters (NCs), such as  $\{M^+ \cdot (OH \cdot H_2O) \cdot H_2O_{n-1}\}$  complex(33-36). The interface state with a characteristic of  $\pi \rightarrow \pi^*$  transition, not only provides an ensemble of intermediate states for bright photoluminescence (PL) emission, but also acts as an alternative reaction channel for electron and proton transfer(21, 22, 31). Thus, we believe that, due to the dosing of Pt atoms, the surface binding of hydroxyl and/or water molecules with Pt cations restructured interface states of  $\{Pt^{\delta+} \cdot (OH \cdot H_2O) \cdot Ag^{\delta+}\}$  as an intermediate, which boosts the reduction of  $Ag^+$  at the interface and promotes subsequent nucleation and growth of Ag NPs with larger size (Fig. 1f). This probably also answers the reason of orientation growth of Ag NPs with varied morphology when different surface ligand or the second metal was introduced in the synthesis(47-50). The above results indicate a new way to synthesize the new metal NPs with varied morphology and/or crystal facets, but beyond the current discussion.

We further evaluated the catalytic performance of bimetallic  $Pt_xAg_{2-x}@DMSNs$  with different compositions in the hydrogenation of 4-NP (Fig.1g). The bimetallic  $Pt_xAg_{2-x}@DMSNs$  exhibit higher activity compared with pure Pt NCs ( $0.065 \text{ min}^{-1}$ ) and Ag NPs ( $0.545 \text{ min}^{-1}$ ).  $Pt_{0.25}Ag_{1.75}@DMSNs$  showed optimal reduction rate at  $1.083 \text{ min}^{-1}$ , which is twice as fast as monometallic Ag NPs ( $0.065 \text{ min}^{-1}$ ) and about 17 times of pure Pt NCs ( $0.065 \text{ min}^{-1}$ ). It also exhibits good stability and reusability that could sustain the conversion of  $\sim 100\%$  within minutes for more than five cycles (Fig. S7). Generally, the size effect, local surface plasmon resonance (LSPR) in Ag-based catalyst and electronic effect of metal centers are responsible for the high reactivity(51). To evaluate the size effect of metal NPs on catalytic performance,  $Ag_x@dmsns$  with different particle size ranging from 1.0-8.0 nm were prepared by controlling metal content (Fig. S4). The catalytic performance exhibits a volcano-like curve that the optimum particle size is ca. 2 nm in  $Ag_{2.0}@DMSNs$ . However, the size of Ag NPs in  $Pt_{0.25}Ag_{1.75}@DMSNs$  with highest activity is biggest about 7.0 nm. Thus, the excellent reactivity of the bimetallic is not caused by size effect. Then, the local surface plasmon resonance (LSPR) effect of Ag in bimetallic catalysts were further explored by ultraviolet-visible (UV-vis) spectra (Fig. S5). The absorption peak of Ag induced by LSPR effect is located at ca. 405 nm. With the decrease of Ag content, the intensity of absorption peak decreased and the position shifts to blue, while the activity showed a volcanic trend. Therefore, the LSPR effect was also unable to explain the promoted activity in bimetallic catalysts, i.e., the metal NP is not true active site for the reduction of 4-NP.

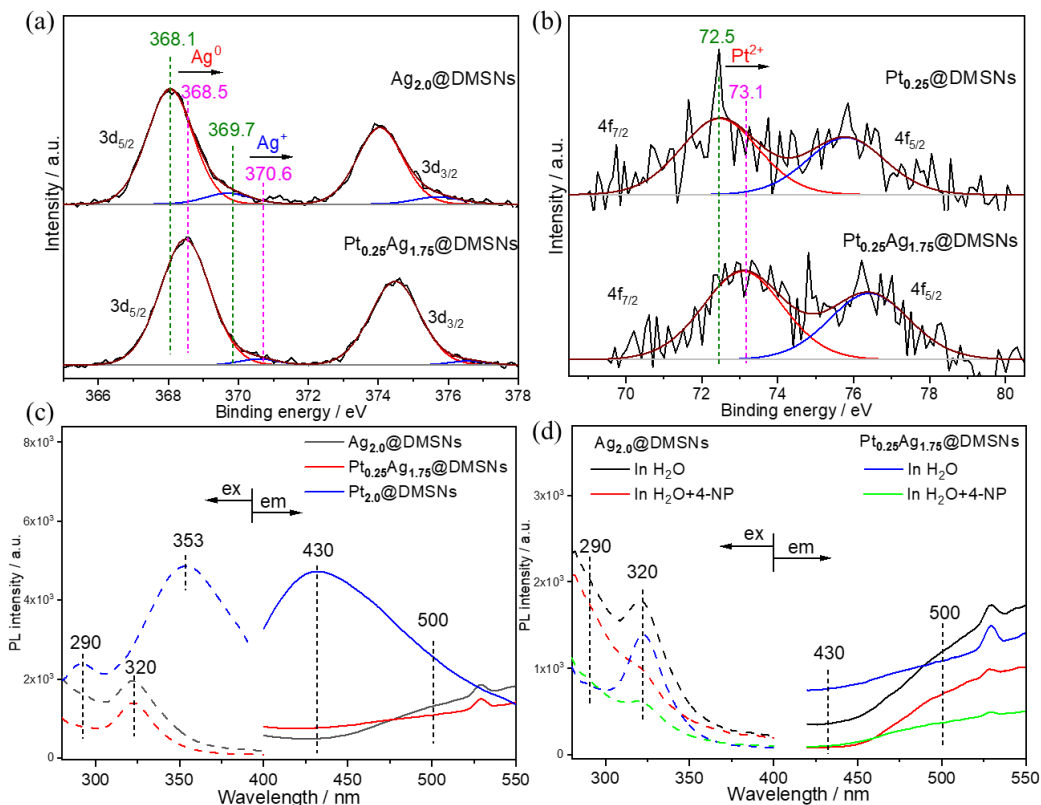


**Figure 2.** Excitation (dash line) and emission spectra (solid line) of Pt, Ag and Pt-Ag bimetal supported DMSNs catalysts in H<sub>2</sub>O (a), and in 4-NP (b).

Since the improved performance in bimetallic have been pervasive attributed to “synergistic effect” arising from Metal-to-Metal direct charge transfer by providing an uneven distribution of electrons, the valence state of single metal and bimetals were determined by XPS (Fig. 2 a, b). The fitting results are summarized in Table S1, S2. In monometallic Ag<sub>2.0</sub>@DMSNs, the components at 368.1 eV and 369.7 eV were assigned to Ag<sup>0</sup> (red) and Ag<sup>+</sup> (blue), respectively. As expected, according to the basic principles of electronegativity (Ag: 1.9; Pt: 2.2), the work function (Ag: 4.26 eV; Pt: 5.65 eV) and redox potential (Ag: 0.8; Pt: 1.2), the electron transfer from Ag to Pt is easier, so the BE of Ag shifted remarkably to a higher value (Ag<sup>0</sup>: 369.7, Ag<sup>+</sup>: 370.6 eV) in bimetallic Pt<sub>0.25</sub>Ag<sub>1.75</sub>@DMSNs. As a result, the electron density of Pt should be more negative with a smaller BE value. On the contrary, counter-intuitively, the BE of Pt<sup>2+</sup> shifted from 72.5 eV to a higher value 73.1 eV remarkably in Pt<sub>0.25</sub>Ag<sub>1.75</sub>@DMSNs indicating the presence of alternative surface states (or channels) for electron release at bimetal nanoscale interface. This differs from the traditional interfacial electron transfer theory via metal-to-metal transfer routes (scheme 1a). Recently, on the surface of nanocluster, especially in monometallic {M<sup>+</sup>•(OH•H<sub>2</sub>O)•H<sub>2</sub>O<sub>n-1</sub>} complex, a new interfacial state (PBIS), stemming from the spatial overlapping of p orbitals of interface atoms, are confirmed exist with the help of steady and ultra-fast absorption and emission spectra(33-36). The interfacial state (PBIS)

not only acted as “electron pool”, but also providing an alternative channel for interfacial electron transfer mediated by proton transfer(21, 22, 31). Thus, we tentatively concluded that the reconstruction of surface states accelerates interfacial electron transfer owing to the dosing of second metal Pt, which has medium coordination ability with hydroxide and/or water molecules.

The absorption and emission features confirmed the presence of interfacial state in bimetallic catalysts. As shown in Figure 1 c, when catalysts are directly dispersed into water solution, the Pt<sub>2.0</sub>@DMSNs catalyst emits the strongest fluorescence at 430 nm with an excitation band at ca. 353 nm (Fig. 1c, blue line and blue dash line). A weaker fluorescence emission centered at 500 nm with an excitation band at ca. 320 nm was observed in Ag<sub>2.0</sub>@DMSNs (Fig. 1c, black line and black dash line). In the recent work, the luminescence centers were identified as p band intermediate states (PBISs), stemming from the space interactions of p orbitals of paired O atoms in {M<sup>+</sup>•(OH•H<sub>2</sub>O)•H<sub>2</sub>O<sub>n-1</sub>} complexes(33-35). For Pt<sub>0.25</sub>Ag<sub>1.75</sub>@DMSNs, the main fluorescence emission is at 500 nm as in pure Ag<sub>2.0</sub>@DMSNs, because Ag is the principal component of bimetallic. Meanwhile, the fluorescence emission at 430 nm increased obviously compared with Ag<sub>2.0</sub>@DMSNs owing to the introduction of trace Pt. Hence, the interfacial state was reconstructed at the surface of bimetals. The observation of the excitation and emission spectrum proves this point (Fig. 2d). When the catalysts are interacted with reactant 4-NP, the PL at ca. 430 nm and 500 nm are less intensified, and concomitantly with a significant increase absorption at ca. 290 nm (Fig. 1d, green line). Obviously, due to the varied overlapping of the two p orbitals of O atoms from hydroxide groups and/or 4-NP, the changes of optical properties indicated the switching of the surface complex from {M<sup>+</sup>•(OH•H<sub>2</sub>O)•H<sub>2</sub>O<sub>n-1</sub>} to {M<sup>+</sup>•(OH•4-NP)•H<sub>2</sub>O<sub>n-1</sub>}. Similar optical properties were recently observed for single Ag NPs catalyst(21).

Clearly, constructing and modifying appropriate interface states by dosing of second Pt metals is the key to control the reaction performance. For the monometallic catalysts of Ag<sub>2.0</sub>@DMSNs and Pt<sub>2.0</sub>@DMSNs, the stronger luminescence intensity of Pt than Ag (Fig. 2c) is probably due to more stable luminous centers are formed on the Pt NPs surface with the strong coordination between Pt and surface OH species(22). Interestingly, the reaction rate of 4-NP reduction is inversely proportional to the stability of the luminescent center, and that Ag<sub>2.0</sub>@DMSNs exhibits better catalytic performance in the conversion of 4-NP to 4-AP (Fig. 1d). Based on Sabatier Principle, this is because too stable interface state on Pt<sub>2.0</sub>@DMSNs prohibits the chemical adsorptions of NaBH<sub>4</sub> and reactant 4-NP, consequently resulting in lower reactivity(22). However, we discovered that, a more stable interface state is necessary in Ag<sub>2.0</sub>@DMSNs by introducing proper amount of interfacial hydroxyl groups into Ag NPs surface(21), which are more conducive to electron and proton transfer, consequently resulting in the promoted



conversion rate of 4-nitrophenol (Fig. S6). Thus, we conclude that, the reaction performance not only depends on the density of surface hydroxyl groups ( $\text{OH}^-$ ) and also the binding strength between hydroxyl groups and metals. For bimetallic  $\text{Pt}_{0.25}\text{Ag}_{1.75}@DMSNs$  catalyst, due to the strong interaction between Pt and  $\text{OH}^-$ , the introduction of trace Pt increased the density of interfacial  $\text{OH}^-$ , which was beneficial to the construction and stabilization of the hydrous hydroxyl related interface state to promote the electron and proton transfer, and without inhibiting the adsorption of  $\text{BH}_4^-$  at the same time.

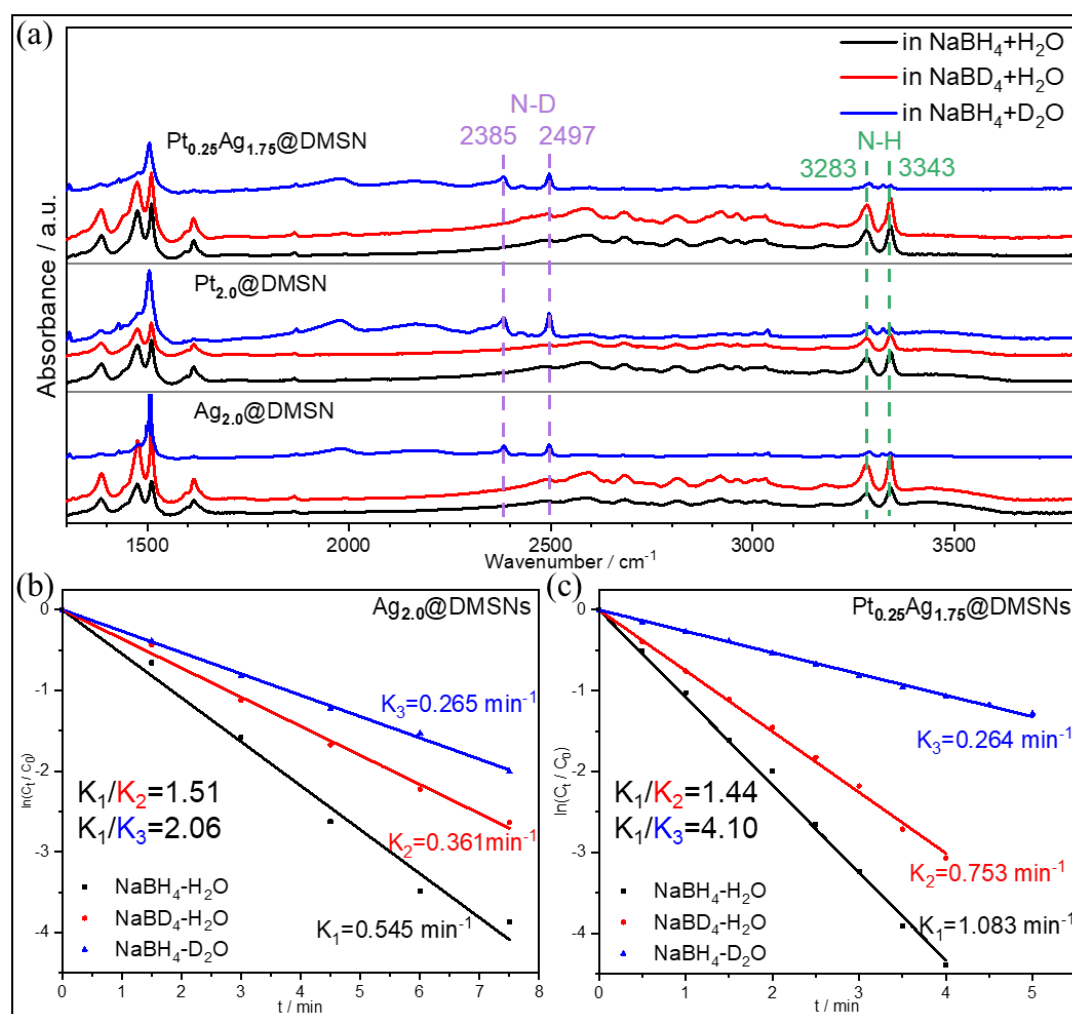


**Figure 3.** (a) FTIR spectra of the final products after the hydride reduction of 4-NP using  $\text{NaBH}_4$  and  $\text{H}_2\text{O}$  (black line),  $\text{NaBD}_4$  and  $\text{H}_2\text{O}$  (red line) and  $\text{NaBH}_4$  and  $\text{D}_2\text{O}$  (blue line). Kinetic isotope effects (KIEs) of  $\text{NaBD}_4$  or  $\text{D}_2\text{O}$  of  $\text{Ag}_{2.0}@DMSNs$  (b) and  $\text{Pt}_{0.25}\text{Ag}_{1.75}@DMSNs$  (c).

Kinetic isotope effects (KIEs) with deuterated reducing agent  $\text{NaBD}_4$  and/or solvent  $\text{D}_2\text{O}$  provides direct experimental evidence on the presence of unique surface states, which promotes the concerned electron and proton transfer, differing from the traditional metal-centered electron and hydride transfer mechanism. The catalytic reduction of 4-NP in Fig. 3b and 3c follows the first-order kinetics as previously reported(29). The reagent ( $k_{\text{NaBH}_4}/k_{\text{NaBD}_4}$ )

and solvent ( $k_{\text{H}_2\text{O}/\text{D}_2\text{O}}$ ) KIE value is 1.51 and 2.06 in monometallic  $\text{Ag}_{2.0}@\text{DMSNs}$ , respectively. In terms of bimetallic  $\text{Pt}_{0.25}\text{Ag}_{1.75}@\text{DMSNs}$ , the KIE value of reagent ( $k_{\text{NaBH}_4/\text{NaBD}_4}$ ) is 1.44 as a similar value as  $\text{Ag}_{2.0}@\text{DMSNs}$ , indicating the cleavage of B-H bond is not rate determined step (RDS) for reduction of 4-NP. Notably, a larger KIE value of solvent ( $k_{\text{H}_2\text{O}/\text{D}_2\text{O}}$ ) is up to 4.10 twice as much as  $\text{Ag}_{2.0}@\text{DMSNs}$ . As we observed, no matter in monometallic or bimetallic catalysts, the dissociation of the B-H bond of borohydride ions and O-H bond of water solvent both involve the reaction kinetics of catalytic hydride reduction of 4-NP(52, 53). Different from the traditional theory that the cleavage of B-H bond mediated by metal was the rate-determining step (RDS)(54)(scheme 1 c), the larger KIE value of solvent ( $k_{\text{H}_2\text{O}/\text{D}_2\text{O}}$ ) than that of reagent ( $k_{\text{NaBH}_4/\text{NaBD}_4}$ ) demonstrates the dissociation of O-H bond of water involving electron transfer and interfacial proton transfer to combine with a nitro group is RDS of this reaction, which further proves that interface state mediated electron and proton transfer mechanism(22, 29). Compared with  $\text{Ag}_{2.0}@\text{DMSNs}$ , the most equal value of  $k_{\text{NaBH}_4/\text{NaBD}_4}$  (1.44) and greatly larger value of  $k_{\text{H}_2\text{O}/\text{D}_2\text{O}}$  (4.10) in  $\text{Pt}_{0.25}\text{Ag}_{1.75}@\text{DMSNs}$ , suggested a suitable interface state are modified, which greatly promoted the concerned electron and proton without the inhibition of adsorption and activation  $\text{BH}_4^-$ .

The analysis of final product of 4-NP reduction by FT-IR spectrum with deuterium isotopic labeling of  $\text{NaBD}_4$  reducer and  $\text{D}_2\text{O}$  solvent provide further evidence on the presence of interface states to mediate concerted electron and proton transfer mechanism on bimetal surface.  $\text{H}_2\text{O}$  is used as the solvent, (Fig. 3a, black and red lines), the transmittance peaks at approximately  $3283$  and  $3343\text{ cm}^{-1}$  are attributed to the N-H bond, indicating the formation of products 4-AP (Figure S7). Although  $\text{NaBD}_4$  is used as the reducing agent, the characteristic peak of FT-IR displays the same feature as that when  $\text{NaBH}_4$  is used. It demonstrates that the hydrogen atoms of  $-\text{NH}_2$  are not from  $\text{BH}_4^-$ (22, 29). However, when  $\text{D}_2\text{O}$  was introduced with  $\text{NaBH}_4$  as a reducer, in striking contrast, the N-H vibration bands vanish and new peaks at  $2385$  and  $2497\text{ cm}^{-1}$  ascribed to the N-D bond are observed (Fig. 3a, blue lines), which suggest the hydrogen source are from the protic solvent water, rather than hydride reducer  $\text{NaBH}_4$ . This indicates that catalytic hydride reduction of 4-NP to 4-AP is not dominated by conventionally accepted metal-centered electron and hydride transfer mechanism, i.e., classical L-H mechanism (Scheme 1a-c), but through a new interface state mediated electron and proton transfer mechanism due to the formation of surface hydrous hydroxyl intermediates. Very recently, on the mono metal catalysts, with the help of  $^1\text{H}$  NMR spectroscopies, once  $\text{BH}_4^-$  were introduced, a new  $\text{H}_3\text{B}$ -water-hydroxyl complex with a triangular configuration and concomitantly with a trapped hydride ( $\text{H}^-$ ) specie was captured (Scheme 1e), and the electron of hydride was very fast transferred to the proton of water (Scheme 1e and f)(22). This quite reasonably answers the KIE of  $\text{NaBD}_4$  and  $\text{D}_2\text{O}$  (Fig. 3b and c), and also

answers the hydrogen origin of the final product of 4-AP (Fig. 3a). Thus, the main role of the second metal of Pt is to construct the surface states for electron and proton transfer, not only to element to tune electronic factors of actives, which answers, even in the absence of metal, the reduction of 4-NP could be efficiently occurred(40).

## Conclusion

In conclusion, a mechanistic study of bimetallic Pt-Ag-catalyzed hydride reduction of 4-NP to 4-AP is presented. Via the investigation of the valence state of the metal and optical spectroscopies, together with reaction kinetic data and kinetic isotope effects, the interface states (PBIS), stemming from space overlapping of p orbitals of O atoms of water-hydroxyl-metal complex ( $\{M^+ \cdot (OH \cdot H_2O) \cdot H_2O_{n-1}\}$ ) are confirmed to be formed on the surface of bimetal. The introduction of trace Pt atoms with moderate coordinate ability to hydroxyl groups regulates the density and interfacial adsorption strength of hydrous hydroxyl groups, which not only accelerates the catalytic hydride reduction of 4-NP, but also promotes the ripening and growth of Ag NPs. Differing from the traditional metal-centered electron and hydride transfer mechanism (L-H mechanism, Scheme 1a-c), the catalytic reduction of 4-NP follows the interfacial concerted electron and proton transfer mechanism via a unique dynamic Pt-OH $\cdot$ H<sub>2</sub>O-Ag intermediates (Scheme 1d-f). The presence of dynamic surface states on the metal surface to direct the concerted electron and proton transfer answers both the kinetic isotope effects (KIE) of D<sub>2</sub>O/H<sub>2</sub>O and hydrogen origin of final product of 4-AP, and probably elucidate the physical reason of abnormal reverse electron transfer in thermal dynamics of bimetal systems(6, 7, 55). The introduction of the concept of interface states reveals the mystery of “synergistic effect” of electron state in bimetallic materials. It opened a new perspective for us to rethink the nature of catalysis and interfacial bonding (or states) and lead to new design principles of heterogeneous catalysts.

## Reference

1. V. R. Stamenkovic *et al.*, Improved Oxygen Reduction Activity on Pt<sub>3</sub>Ni(111) via Increased Surface Site Availability. *Science* **315**, 493-497 (2007).
2. M. Sankar *et al.*, Designing bimetallic catalysts for a green and sustainable future. *Chem Soc Rev* **41**, 8099-8139 (2012).
3. X. Peng, Q. Pan, G. L. Rempel, Bimetallic dendrimer-encapsulated nanoparticles as catalysts: a review of the research advances. *Chem Soc Rev* **37**, 1619-1628 (2008).
4. J. Zhang, G. Chen, D. Guay, M. Chaker, D. Ma, Highly active PtAu alloy nanoparticle catalysts for the reduction of 4-nitrophenol. *Nanoscale* **6**, 2125-2130 (2014).
5. Z. Wu, Anti-galvanic reduction of thiolate-protected gold and silver nanoparticles. *Angew Chem Int Ed Engl* **51**, 2934-2938 (2012).
6. I.-R. Jeon *et al.*, Spin crossover or intra-molecular electron transfer in a cyanido-bridged

- Fe/Co dinuclear dumbbell: a matter of state. *Chemical Science* **4**, (2013).
7. Z. Gan, N. Xia, Z. Wu, Discovery, Mechanism, and Application of Antigalvanic Reaction. *Acc Chem Res* **51**, 2774-2783 (2018).
  8. T. S. Kim, J. Gong, R. A. Ojifinni, J. M. White, C. B. Mullins, Water Activated by Atomic Oxygen on Au(111) to Oxidize CO at Low Temperatures. *J. Am. Chem. Soc.* **128**, 6282-6283 (2006).
  9. R. A. Ojifinni *et al.*, Water-Enhanced Low-Temperature CO Oxidation and Isotope Effects on Atomic Oxygen-Covered Au(111). *J. Am. Chem. Soc.* **130**, 6801-6812 (2008).
  10. G. M. Mullen, J. Gong, T. Yan, M. Pan, C. B. Mullins, The Effects of Adsorbed Water on Gold Catalysis and Surface Chemistry. *Topics in Catalysis* **56**, 1499-1511 (2013).
  11. G. Chen *et al.*, Interfacial Effects in Iron-Nickel Hydroxide-Platinum Nanoparticles Enhance Catalytic Oxidation. *Science* **344**, 495-499 (2014).
  12. Y. Zhai *et al.*, Alkali-Stabilized Pt-OH<sub>x</sub> Species Catalyze Low-Temperature Water-Gas Shift Reactions. *Science* **329**, 1633-1636 (2010).
  13. M. Yang *et al.*, Catalytically active Au-O(OH)<sub>x</sub> species stabilized by alkali ions on zeolites and mesoporous oxides. *Science* **346**, 1498-1501 (2014).
  14. M. Yang *et al.*, A common single-site Pt(II)-O(OH)<sub>x</sub> species stabilized by sodium on "active" and "inert" supports catalyzes the water-gas shift reaction. *J Am Chem Soc* **137**, 3470-3473 (2015).
  15. W. Deng *et al.*, Crucial Role of Surface Hydroxyls on the Activity and Stability in Electrochemical CO<sub>2</sub> Reduction. *J Am Chem Soc* **141**, 2911-2915 (2019).
  16. C. Yang *et al.*, Hydroxyl-mediated ethanol selectivity of CO<sub>2</sub> hydrogenation. *Chem Sci* **10**, 3161-3167 (2019).
  17. Z. J. Zhao *et al.*, Hydroxyl-Mediated Non-oxidative Propane Dehydrogenation over VO<sub>x</sub>/γ-Al<sub>2</sub>O<sub>3</sub> Catalysts with Improved Stability. *Angew Chem Int Ed Engl* **57**, 6791-6795 (2018).
  18. C. Hu *et al.*, Synergism of Geometric Construction and Electronic Regulation: 3D Se-(NiCo)<sub>Sx</sub>/(OH)<sub>x</sub> Nanosheets for Highly Efficient Overall Water Splitting. *Adv Mater* **30**, e1705538 (2018).
  19. G. Liu *et al.*, Platinum-Modified ZnO/Al<sub>2</sub>O<sub>3</sub> for Propane Dehydrogenation: Minimized Platinum Usage and Improved Catalytic Stability. *ACS Catalysis* **6**, 2158-2162 (2016).
  20. Y. Wang *et al.*, Chemoselective Hydrogenation of Nitroaromatics at the Nanoscale Iron(III)-OH-Platinum Interface. *Angew Chem Int Ed Engl* **59**, 12736-12740 (2020).
  21. X.-D. Hu, B.-Q. Shan, R. Tao, T.-Q. Yang, K. Zhang, Interfacial Hydroxyl Promotes the Reduction of 4-Nitrophenol by Ag-based Catalysts Confined in Dendritic Mesoporous Silica Nanospheres. *The Journal of Physical Chemistry C* **125**, 2446-2453 (2021).
  22. B. Q. Shan, J. F. Zhou, M. Ding, X. D. Hu, K. Zhang, Surface electronic states mediate concerted electron and proton transfer at metal nanoscale interfaces for catalytic hydride reduction of -NO<sub>2</sub> to -NH<sub>2</sub>. *Phys Chem Chem Phys* **23**, 12950-12957 (2021).
  23. S. M. Gopal *et al.*, Conformational Preferences of an Intrinsically Disordered Protein Domain: A Case Study for Modern Force Fields. *J Phys Chem B* **125**, 24-35 (2021).
  24. Y. Wang *et al.*, Highly Active Supported Pt Nanocatalysts Synthesized by Alcohol Reduction towards Hydrogenation of Cinnamaldehyde: Synergy of Metal Valence and Hydroxyl Groups. *Chem Asian J* **10**, 1561-1570 (2015).
  25. S. Bhogeswararao, D. Srinivas, Intramolecular selective hydrogenation of cinnamaldehyde

- over CeO<sub>2</sub>–ZrO<sub>2</sub>-supported Pt catalysts. *Journal of Catalysis* **285**, 31-40 (2012).
26. C.-Y. Hsu *et al.*, Effect of Electron Density of Pt Catalysts Supported on Alkali Titanate Nanotubes in Cinnamaldehyde Hydrogenation. *J. Phys. Chem. C* **114**, 4502-4510 (2010).
  27. L. Wang *et al.*, Single-site catalyst promoters accelerate metal-catalyzed nitroarene hydrogenation. *Nat Commun* **9**, 1362 (2018).
  28. R. Grzeschik *et al.*, On the Overlooked Critical Role of the pH Value on the Kinetics of the 4-Nitrophenol NaBH<sub>4</sub> -Reduction Catalyzed by Noble Metal Nanoparticles (Pt, Pd, Au). *The Journal of Physical Chemistry C* **124**, 2939–2944 (2020).
  29. Y. Zhao *et al.*, Mechanistic Study of Catalytic Hydride Reduction of –NO<sub>2</sub> to –NH<sub>2</sub> Using Isotopic Solvent and Reducer: The Real Hydrogen Source. *The Journal of Physical Chemistry C* **123**, 15582-15588 (2019).
  30. S. Shirin, S. Roy, A. Rao, P. P. Pillai, Accelerated Reduction of 4-Nitrophenol: Bridging Interaction Outplays Reducing Power in the Model Nanoparticle-Catalyzed Reaction. *The Journal of Physical Chemistry C* **124**, 19157-19165 (2020).
  31. R. T. e. al., Surface Molecule Manipulated Pt/TiO<sub>2</sub> catalysts for Selective Hydrogenation of Cinnamaldehyde. *ChemRxiv*, (2021).
  32. K. Qu, Y. Zheng, S. Dai, S. Z. Qiao, Graphene oxide-polydopamine derived N, S-codoped carbon nanosheets as superior bifunctional electrocatalysts for oxygen reduction and evolution. *Nano Energy* **19**, 373-381 (2016).
  33. T. Yang *et al.*, P band intermediate state (PBIS) tailors photoluminescence emission at confined nanoscale interface. *Communications Chemistry* **2**, (2019).
  34. T. Q. Yang *et al.*, Origin of the Photoluminescence of Metal Nanoclusters: From Metal-Centered Emission to Ligand-Centered Emission. *Nanomaterials (Basel)* **10**, (2020).
  35. T.-Q. Y. Xiao-Dan Hu, 1 Bing-Qian Shan, 1 Bo Peng, 1 Kun Zhang, Topological excitation of singly hydrated hydroxide complex in confined sub-nanospace for bright color emission and heterogeneous catalysis. *ChemRxiv* (2020).
  36. J. Zhou *et al.*, Structural Water Molecules Confined in Soft and Hard Nanocavities as Bright Color Emitters <https://doi.org/10.1021/acspchemau.1c00020>.
  37. T. Q. Yang *et al.*, Caged structural water molecules emit tunable brighter colors by topological excitation. *Nanoscale* **13**, 15058-15066 (2021).
  38. M. Kohantorabi, M. R. Gholami, AgPt nanoparticles supported on magnetic graphene oxide nanosheets for catalytic reduction of 4 - nitrophenol: Studies of kinetics and mechanism. *Applied Organometallic Chemistry* **31**, (2017).
  39. C. Wang *et al.*, Highly Efficient Transition Metal Nanoparticle Catalysts in Aqueous Solutions. *Angew Chem Int Ed Engl* **55**, 3091-3095 (2016).
  40. H. Liu *et al.*, Nitrogen-Doped Graphene Quantum Dots as Metal-Free Photocatalysts for Near-Infrared Enhanced Reduction of 4-Nitrophenol. *ACS Applied Nano Materials* **2**, 7043-7050 (2019).
  41. K. Zhang *et al.*, Facile large-scale synthesis of monodisperse mesoporous silica nanospheres with tunable pore structure. *J Am Chem Soc* **135**, 2427-2430 (2013).
  42. P. Hao, B. Peng, B.-Q. Shan, T.-Q. Yang, K. Zhang, Comprehensive understanding of the synthesis and formation mechanism of dendritic mesoporous silica nanospheres. *Nanoscale Advances* **2**, 1792-1810 (2020).
  43. T.-Q. Yang *et al.*, Interfacial electron transfer promotes photo-catalytic reduction of

- 4-nitrophenol by Au/Ag<sub>2</sub>O nanoparticles confined in dendritic mesoporous silica nanospheres. *Catalysis Science & Technology* **9**, 5786-5792 (2019).
44. Y. Zong *et al.*, Spatial and chemical confined ultra-small CsPbBr<sub>3</sub> perovskites in dendritic mesoporous silica nanospheres with enhanced stability. *Microporous and Mesoporous Materials* **302**, (2020).
45. H. Chen *et al.*, Effect of Atomic Ordering Transformation of PtNi Nanoparticles on Alkaline Hydrogen Evolution: Unexpected Superior Activity of the Disordered Phase. *The Journal of Physical Chemistry C* **124**, 5036-5045 (2020).
46. C. Chen *et al.*, Highly Crystalline Multimetallic Nanoframes with Three-Dimensional Electrocatalytic Surfaces. *Science* **343**, 1339-1343 (2014).
47. R. R. da Silva *et al.*, Facile Synthesis of Sub-20 nm Silver Nanowires through a Bromide-Mediated Polyol Method. *ACS Nano* **10**, 7892-7900 (2016).
48. Z. He, Y. Yang, H. W. Liang, J. W. Liu, S. H. Yu, Nanowire Genome: A Magic Toolbox for 1D Nanostructures. *Adv Mater* **31**, e1902807 (2019).
49. M. Yang, Z. D. Hood, X. Yang, M. Chi, Y. Xia, Facile synthesis of Ag@Au core-sheath nanowires with greatly improved stability against oxidation. *Chem Commun (Camb)* **53**, 1965-1968 (2017).
50. Y. Sun, Y. Xia, Mechanistic Study on the Replacement Reaction between Silver Nanostructures and Chloroauric Acid in Aqueous Medium. *J. AM. CHEM. SOC.* **126**, 3892-3901 (2004).
51. J. Quiroz *et al.*, Controlling Reaction Selectivity over Hybrid Plasmonic Nanocatalysts. *Nano Lett* **18**, 7289-7297 (2018).
52. R. E. Davis, E. Bromels, C. L. Kibby, Boron Hydrides. III. Hydrolysis of Sodium Borohydride in Aqueous Solution. *J. Am. Chem. Soc.* **84**, 885-892 (1962).
53. R. E. Dessy, E. Grannen, The Kinetics and Mechanism of the Reaction of Borohydrides with Weak Acids<sup>1</sup>. *J. Am. Chem. Soc.* **83**, 3953-3958 (1961).
54. S. Fountoulaki *et al.*, Mechanistic Studies of the Reduction of Nitroarenes by NaBH<sub>4</sub> or Hydrosilanes Catalyzed by Supported Gold Nanoparticles. *ACS Catalysis* **4**, 3504-3511 (2014).
55. B. Peng *et al.*, Physical Origin of Dual-Emission of Au–Ag Bimetallic Nanoclusters. *Frontiers in Chemistry* **9**, (2021).